International Research Journal of Engineering and Technology (IRJET) e-ISSN: 2395-0056
Volume: 09 Issue: 10 | Oct 2022 www.irjet.net p-ISSN: 2395-0072

Equilibrium, Kinetics and Thermodynamic studies for Removal of Methy Red dye by Green Synthesized Copper Oxide Nanoparticles (Adenanthera Pavonina leaves)

V.Anbarasan[1], and K. Arivalagan[2]

[1]Department of Chemistry, DMI college of Engineering,Chennai-600123..
[2]Department of Chemistry, Govt Arts College for Men(A) Nandanam,Chennai.600035.

ABSTRACT

Nanoparticles are the spearheads of the rapidly expanding field of nanotechnology. Development of the green synthesis has gained extensive attention as a reliable, sustainable and eco-friendly protocol for synthesizing a wide range of metal and metal oxide nanoparticles. The present study is to undertake Equilibrium, Kinetics and Thermodynamic studies for Removal of Methyl Red dye by Green Synthesized Copper Oxide Nanoparticles (Adenanthera Pavonina leaves). The synthesized copper oxide nanoparticles were characterized by Ultraviolet Vis spectroscopy (UV-Vis), X-ray Diffraction (XRD), Fourier Transform Infrared Spectroscopy (FT-IR), Scanning Electron Microscope (SEM), Transmission Electron Microscope (TEM), Energy Dispersive X-ray (EDX), and Dynamic Light Scattering (DLS). Adsorption parameters such as Initial dye concentration, Adsorbent dosage, pH, contact time, and Temperature were studied. Adsorption isotherm has been used to test the adsorption data (Langmuir, Freundlich, Temkin), Kinetics and thermodynamic parameters were also calculated. In addition, results indicate that the adsorption equilibrium data well fitted with Langmuir isotherm compared to Freundlich and Temkin isotherm. The adsorption kinetics shows good agreement of pseudo second order kinetic model. Moreover, the negative value of ΔG^o reveals the spontaneous nature of the adsorption process and the negative value of ΔH^o indicates the adsorption process exothermic and the positive values of ΔS^o suggest increasing randomness of the adsorbent solution interface during the adsorption process of APL CuONPs. The green chemistry approach used in the present work for the synthesize of copper oxide nanoparticles is simple, cost effective, and good alternative method. The green synthesized copper oxide nanoparticles with high dye adsorption capacity might be a suitable option for dye removal from coloured aqueous solution. CuO nanoparticle prepared from above mentioned routes is expected to have more extensive applications such as Chemical sensor, Catalytic, Gas sensor, Semiconductor etc. This process is an economical method with respective to energy, time and its simplicity. Through this method a large scale of Green synthesized Copper Oxide Nanoparticles was produced.

Keywords: *Adenanthera Pavonina* leaves, Extract, Copper oxide nanoparticles, Characterization, Dye, Adsorption, Kinetics, Thermodynamics.

Correspondences: V. Anbarasan, Tel: +91-9003955707, Email: vkanbu51@gmail.com

1. INTRODUCTION

Nanotechnology can be defined as the manipulation of mater through certain chemical and physical process to create materials with specific properties which can be use particular application [1]. A nanoparticle can be defined as a microscopic particle that has at least one dimension less than 100 nm in size [2]. Nanotechnology generally involves the application of extremely small particles that are used across all field of science including chemistry, biology, medicine and material science [3-4]. Nanoparticles are the spearheads of the rapidly expanding field of nanotechnology. Different types of nanoparticles with desired shape and size have been fabricated using various approaches like physical, chemical and biological techniques [5].

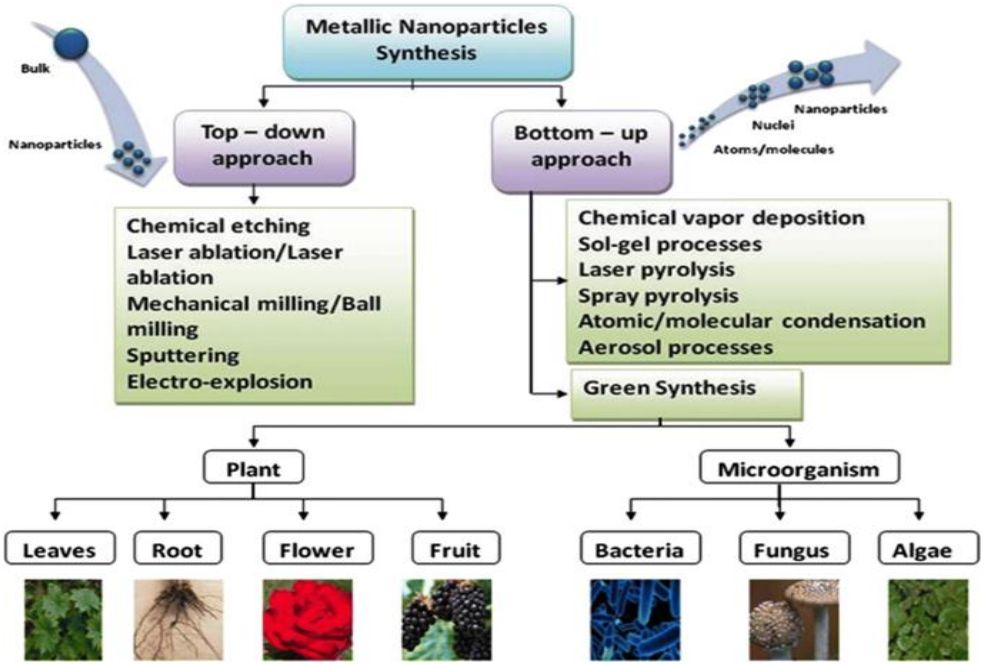

Fig. 1. Schematic diagram of synthesis of nanoparticles

The biological method which is represented as an alternative to chemical and physical methods, provides an environmentally friendly way of synthesizing nanoparticles. Moreover, this method does not require expensive, harmful and toxic chemicals. Metallic nanoparticles with various shapes, sizes contents and physio chemical properties can be synthesized the biological method actively used in recent years. Traditional methods are used from past many years but researches have proved that the green methods are more effective for the generation of NPs with advantage of less chances of failure, low cost and ease of characterization.[6]. In the green synthesis method in which nanoparticles with biocompatibility are produced these agents are naturally present in the employed biological organism. Synthesis can be done in one step using biological organism such as Bacteria, Actinobacteria, yeast, molds, algae, and plants (or) their products**.**

The plants are considered to be more suitable compared to microbes for green synthesis of nanoparticles as they are non-pathogenic and various pathways are thoroughly researched. The plants (or) plants extract, which act as reducing and capping agents for nanoparticle synthesis, are more advantageous over other biological process [7]. Because they eliminate the elaborated process of culturing and maintaining of the cell and can also be scaled up for large scale nanoparticle synthesis is preferred because it is cost-effective, environment-friendly, a single step method for bio synthesis process and safe for human therapeutic uses. different parts of plant materials such as extracts. Fruit, fruit peels, bark, root, leaves, and tubers [8]. Plants which have great potential for detoxification, reduction and accumulation of metals are promising fast and economical in removing metal-borne pollutants. Metallic nanoparticles having various morphological characteristics can be produced intra cellularly and extra cellularly. With the materials present in the plant extract such as sugar, flavonoid, protein, enzyme, polymer, and genie acid acting as a reducing agent take charge in bio induction of metal ions into nanoparticles [9-13].

Metal and metal oxide nanomaterials prepared from earth-abundant and inexpensive metals have attracted considerable attention because of their prospect as viable alternatives to the expensive metal-based catalysts used in many conventional chemical processes [14] Nanomaterial's exhibit activities which are different from those of the corresponding bulk materials because of their size and shape-dependent physicochemical and optoelectronic properties [15]. The catalytic activity of nanomaterials represents a rich resource for chemical processes, employed both in industry and in academia. The great interest in catalysis using nanomaterials has prompted the synthesis and investigation of a diverse range of highly functionalized nanoparticles (NPs), including metal oxide nanostructures [16-20]. Some of the distinguish reported types of

nanoparticles includes photochromatic nanoparticles, polymer coated nanoparticles, metal oxide nanoparticles, FeO, CuO, MgO, ZnO, FeNPs, AuNPs, AgNPs, PdNPs [21-23].

Among the various metals like Cu based nanomaterials which are cheap and environmentally friendly are especially attractive in this context due to the high abundance of Cu in nature and the available simple and straightforward techniques to synthesize these nanomaterials. The present green method for the synthesis of CuO nanoparticles is simple, mild, and environmentally friendly. Green synthesis of CuO nonoparticles could also be extended to fabricate other, industrially important metal oxides.

Water conservation is one of the important environmental issues affecting both human being and the earth [24]. Dyes are among the major contributors in water pollution [25]. Wastewater from textile, cosmetic, printing, dyeing, food industry, paper making industries is polluted by dyes. Discharge of the coloured effluents presents a major environmental problem for developing countries because of their toxic and carcinogenic effects on living beings [26]. The annual production of synthetic organic dyes is more than 700,000 tons throughout the world. Besides different industries utilize more than 10,000 different dyes, dyestuff, and pigments [27]. Therefore, many methods such as physical, chemical coagulation and biological treatment have been developed for the removal of dye pollutions from wastewater before being discharge into the environment [28-29]. Among the available technologies for the dye removal adsorption is a selective one with a high efficiency [30-34]. Compare with other technologies it is cost effective better assigned and has a high degree of accessibility and capability in dye removal [35-36].

In the present study copper oxide nanoparticles (CuONPs) were synthesized using *Adenanthera Pavonina* leaves and used for removal Methyl red dye.

2.MATERIAL AND METHODS

2.1 Materials

All chemicals used were of analytical reagent without any further purification in addition to deionised water, copper chloride dihydrate ($CuCl_2.2H_2O$), Sodium hydroxide (NaOH), hydrochloric acid (HCl), and ethanol (C_2H_5OH. Methyl Red (MR) is an azo dye (Known as (2-{E)-[-4-(dimethylamenophenyl] diazinyl} benzoic acid) as well, it is a pH indicator, it is yellow in pH more than 6.2 red in pH values under 4.4 and orange in between. It was selected as model system due to its intense colour in aqueous system and biodegradability because of benzene rings.

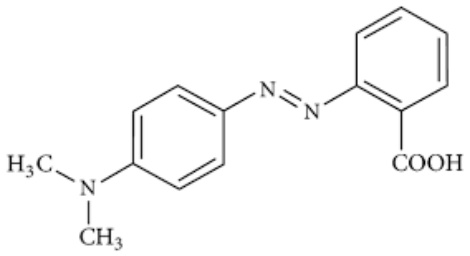

Fig. 2: Molecular structure of Methyl Red (MR)

The molecular structure of Methyl red is depicted in Fig.2 [37]. The chemical formula of methyl red is $C_{15}H_{15}N_3O_2$ with molecular weight (269.31 g/mol λ_{max} = 417nm) [38].

2.2 METHODS

2.2.1 Preparation of Adenanthera Pavonina leaves Extract

The *Adenanthera Pavonina* leaves were collected from Ashok Nagar, Chennai. The fresh tuber was washed several times with tap water followed by distilled water to remove the dust particles. The clean and fresh sources are dried in a shaded

place at room temperature for 10 to 15 days and then the leaves were pulverized using commercial blender. The fine powdered was stored at room temperature for further use. In a 250 ml of conical flask 10 gm of tuber powder were taken and to this 100 ml of double distilled water is added and it is heated at 80°C for 30 minutes. Then the solution was filtered using Whatman filter paper and kept aside for further process. The obtained extract in pale brown colour and adjust the pH at 11 by adding 0.1M of sodium hydroxide solution.

2.2.2 Preparation of Copper Oxide Nanoparticles

In a 250 ml conical flask, 50 ml of *Adenanthera Pavonina* leaves extract was taken and to this 100 ml of 0.1 M $CuCl_2.2H_2O$ solution is added slowly at room temperature under static conditions. The colour change of the reaction was observed and the time taken for the changes was noted. The solution colour changes immediately from pale brownish to yellowish grey colour indicating the formation of copper oxide nanoparticles (CuONP). Further the solution is centrifuged and precipitated is extracted and dried in electrical oven for 24 hours at 100°C. the dried sample kept in muffle furnace for 4 hours at 500°C. the green synthesised CuONPs is formed at uniform particle size and stored for further characterisation and uses.

2.3 Preparation of Adsorbate

The synthetic dye such as Methyl Red (MR) were purchased from kevin laboratories in Chennai. A stock solution of (1000mg/L) was prepared by dissolving 1.0 g of dye distilled water. Distilled water was used for preparing all the solution and reagents.

2.4 CHARACTERIZATION OF COPPER OXIDE NANOPARTICLES

2.4.1 UV-Visible spectrophotometer analysis

Synthesized CuO nanoparticles were subjected to UV-Vis spectroscopy analysis, which confirms the formation of nanoparticles in the initial stage. The CuO nanoparticles synthesized were subjected to scan UV-Vis spectrophotometer in the range 190 nm - 800 nm using Elico SL210 UV VIS Spectrophotometer.

2.4.2. FT-IR Spectroscopic analysis

The plant extract and green synthesized CuO nanoparticles were characterized by FT-IR spectrometer. The spectroscopic technique is based on the analysis of peaks at certain wave numbers. FT-IR data indicates the presence of functional groups in the plant extract and synthesized nanoparticles. The FT-IR analysis carried out in the frequency range of 4000 - 400 cm^{-1} using Perkin Elmer instrument.

2.4.3. X-ray diffraction analysis (XRD)

X-ray diffractometer (lakjdf) was used to study the average particle size and crystalline nature of the synthesized adsorbents. The diffraction pattern was obtained by using CuKα radiation with wavelength of λ=1.541A°. The scanning was done in 2θ value range of 4° to 80° at 0.02 min^{-1} and one second time constant.

2.4.4. Scanning Electron Microscopic (SEM)

The SEM analysis provide the details about surface morphology, porosity and particle size distribution of the adsorbents. The surface morphology of the synthesized CuO nanoparticles was recorded using Hitachi instrument

2.4.5. Energy Dispersive X-ray Spectroscopy (EDX or EDAX)

EDX is an analytical technique used for the elemental analysis of a adsorbent and it depends on the interaction between known source of X-ray excitation and the Adsorbent. The elemental composition of the adsorbent was determined with the help of elemental analyser (CE-440 elemental analyser).

2.4.6 Transmission Electron Microscope (TEM)

TEM is regarded as the best among other electron microscopy techniques for the determination of particle size and morphological identities of CuONPs and other metal nanoparticle

2.4.7. Dynamic Light Scattering analysis (DLS)

DLS is an extensively used technique for determining the hydrodynamic diameter of nanoparticles established on the Brownian movement of particles in the suspension

2.5 Batch adsorption experiments

The experiment was carried out by the batch adsorption method. the removal of dyes was studied various temperature (298K,308K,318K,328k) using the batch technique to investigate the effect of operational parameters such as pH, initial dye concentration, adsorbent dosage, contact time, and solution temperature. The isotherm study was carried out with different initial dye concentration of dyes from 10 to 70mg/L constant and carefully arranged in the orbital shaker and agitation at 150rpm speed for 30 minutes. The adsorbent dosage was checked from 0.2 to 1.0g for better adsorption. The kinetic study was done by varying time from 30 to 150 minutes, for the thermodynamic study temperature from 298 to 328K. the CuONPs solution was separated by centrifugation at 2000rpm for 10 minutes. Residual concentration of dye was determined UV-visible spectrophotometer at respective wavelength. The percentage of dye removal from solution was calculated following

The percentage of MR adsorbed was determine based on the following formula

$$\% \text{ removal } = \frac{(Co - Ce)}{Co} X\ 100 \qquad Eq.(1)$$

The maximum MR uptake q_e (in mg g^{-1}) was calculated as shown below

$$\text{qe} = \frac{(Co - Ce)V}{M} \qquad Eq.(2)$$

where C_o and C_e are initial and final MR concentration of in mg 1^{-1}, respectively W is the amount of CuONP (in g) and V is the volume of MR solution.

3. RESULTS AND DISCUSSION

3.1. Characterization study of Copper Oxide Nanoparticles.

3.1.1. UV- vis Absorption Spectroscopy for copper oxide Nanoparticles.

The Green approach for the formation of copper oxide nanoparticles using *Adenanthera Pavonina* leaves extract was reported. Formation of copper oxide nanoparticle were confirmed by UV-vis spectrophotometry. Fig 3. shows the UV-Vis absorption spectrum of copper oxide nanoparticle. The adsorption spectrum was recorded for the sample in the range of 200 – 800 nm. The spectrum showed the absorbance peak at 286 nm corresponding to the characteristic band of copper oxide nanoparticle [39].

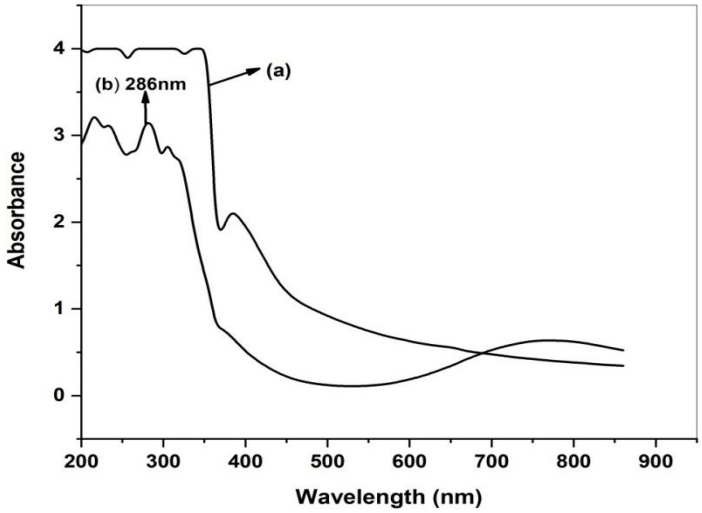

Fig 3. UV-visible adsorption spectrum of a) APL extract and b) APL CuONPs

3.1.2. X-ray Diffraction

The x-ray diffraction (XRD) study was undertaken to Determine and confirm the crystalline structure of synthesized CuONPs. Fig (4) Shows the appearance of diffraction pattern at 2θ= 33.3, 35.4, 38.8, 48.7, 58.3, 61.8, 66.28 and 68.0 which are assigned to the planes (110), (022), (111), (200), (202), (020), (202), (022) respectively of monoclinic phase CuONPs. No characteristic peak due to any impurity was observed in the diffraction grams Suggesting the formation of pure crystalline CuO.

The average size of the CuO was calculated by using the Debye-Scherer Equation (3) [40]. A sharp peak at 20=35.4 and 38.8 with the diffraction of the (022) and (111) plane indicates that confirmation of CuONPs. The average crystallite size in the samples of CuONPs is below 21nm.

$$D = 0.9\lambda / \beta \cos \theta \qquad \text{Eq. (3)}$$

Where λ is the wavelength of the x-ray radiation (0.154nm), θ is the Diffraction angle and β is the full width at half maximum

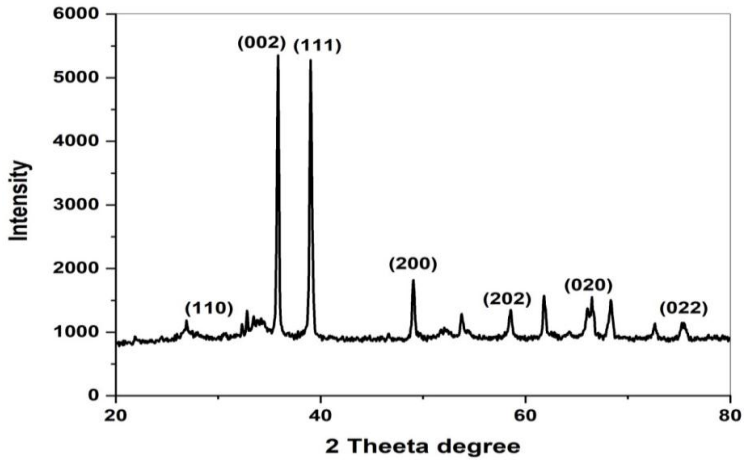

Fig 4: X-ray diffraction pattern of *Adenanthera Pavonina* leaves extract- mediated synthesized CuONPs

3.1.3 Fourier Transform Infrared (FT-IR) Spectroscopy.

FTIR spectroscopy analysis also revealed the possible biomolecules and functional group responsible for capping or stabilizing of the synthesized CuONPs were expressed in fig (5a, 5b). Taking the spectrum of tuber Extract as control the involvement of different functional groups of *Adenanthera Pavonina* leaves extract in reducing and stabilizing process of nanoparticles synthesis was evaluated. Absorbance bands at 3451, 2080, 1625, and 729 cm^{-1} were observed in the spectrum of *Adenanthera Pavonina* leaves extract. A broad band at 3451 cm^{-1} was due to the O-H stretching of alcohol compounds. The peaks at 2080 and 1625 cm^{-1} are Containing -NH_2 group and C=O groups of flavonoids [41-42]. 775 cm^{-1} is containing C-H bonds. FTIR spectrum of CuONP for the peak appeared at 3742, 2116, 1013, 709, and 517 cm^{-1}. The peaks at 3742, 2116 and 1013 cm^{-1} corresponding to hydroxyl group (-OH) Stretching, hydroxyl (-OH) bending and C-O stretching respectively. The Narrow bands at 517 confirm the formation of CuONPs.

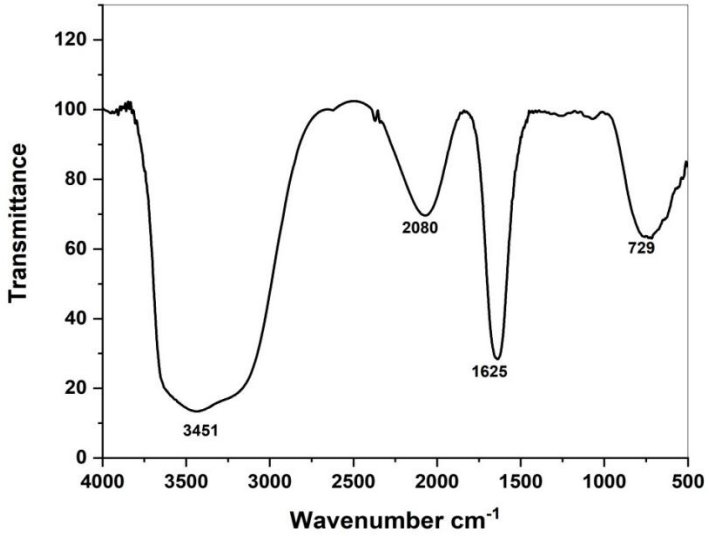

Fig 5a. FTIR spectrum of APL extract

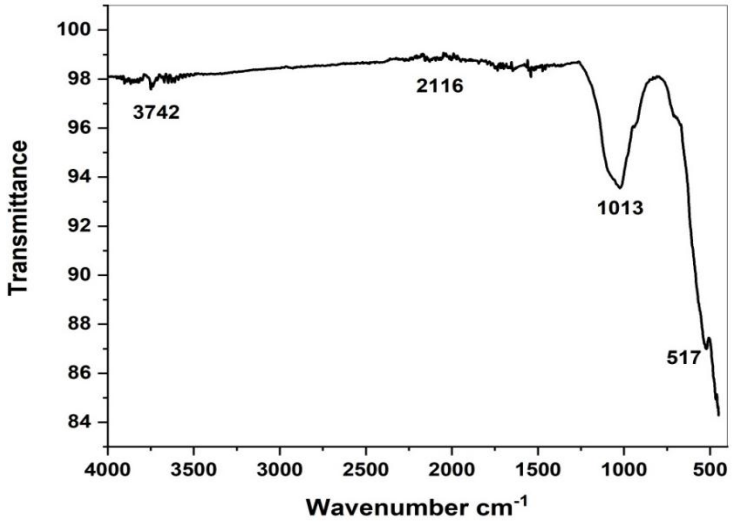

Fig 5b. FTIR spectrum of APL green synthesized CuO NPs

3.1.4. Scanning Electron Microscope (SEM)

The morphology of CuO nanoparticles studied by SEM analysis. Fig (6) showa the surface morphology of the copper oxide nanoparticles was observed in the SEM image. It seems that the diameter of CuO nanoparticles range between 60-80 nm as calculated by image J programme [43].

3.1.5. Energy dispersive X-ray Diffractive (EDX) analysis

The Energy Dispersive X-ray (EDX) study was carried out for the green synthesized CuO nanoparticles to know about the elemental composition. EDX confirm the presence of Cu and O signals of CuO nanoparticles as shown in fig 7 and table 1. The elemental analysis of nanoparticles yields Cu 78.07% and 21.93% of oxygen which process that the produce nanoparticles is in its highest purified form [44].

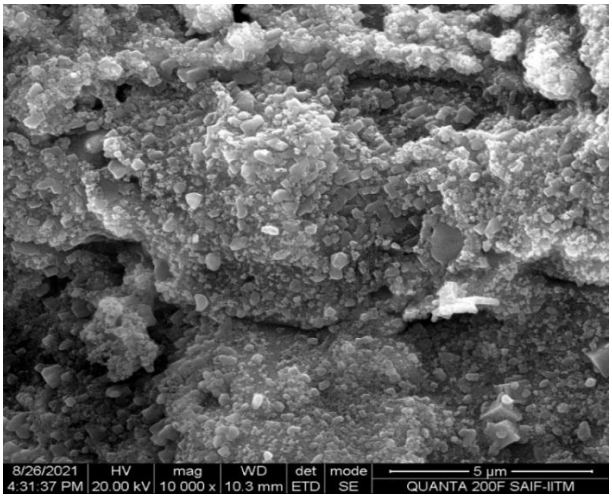

Fig 6. SEM image of Green synthesized APL copper oxide nanoparticles.

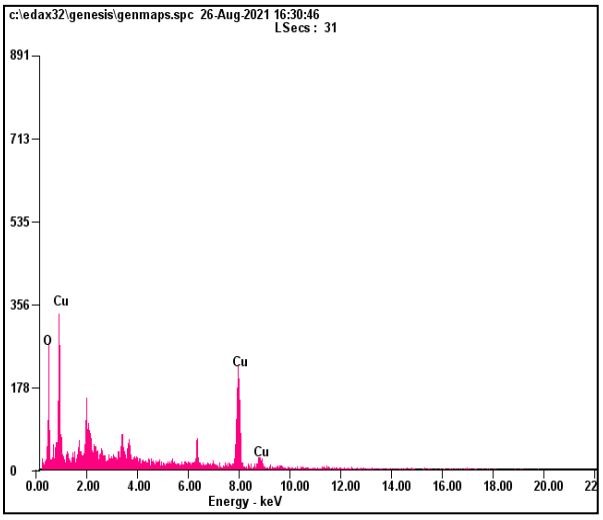

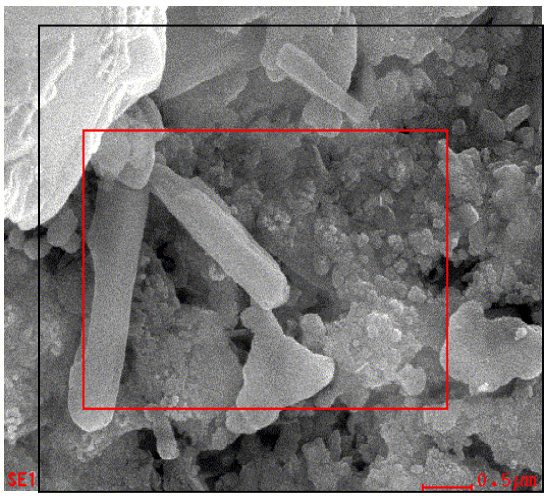

Fig 7 Shows EDX spectrum of APL CuO nanoparticle

Table 1: EDX analysis for synthesized copper oxide nanoparticles.

S.NO	Element	Weight (%)
1.	Cu	78.07
2.	O	21.93

3.1.6 Transmission Electron Microscope (TEM)

The detailed morphological and size analyses of green synthesized copper oxide nanoparticles were studied using electron microscope and results shown in fig 8. The TEM image reveals that the biosynthesis CuONPs wee agglomerated which are interconnected to each other and spherical in shape which is also in agreement with result obtained from SEM. The estimate the particle is found to be between 10-60 nm. The particle size calculated by histogram. The particle size determined TEM close to XRD [45].

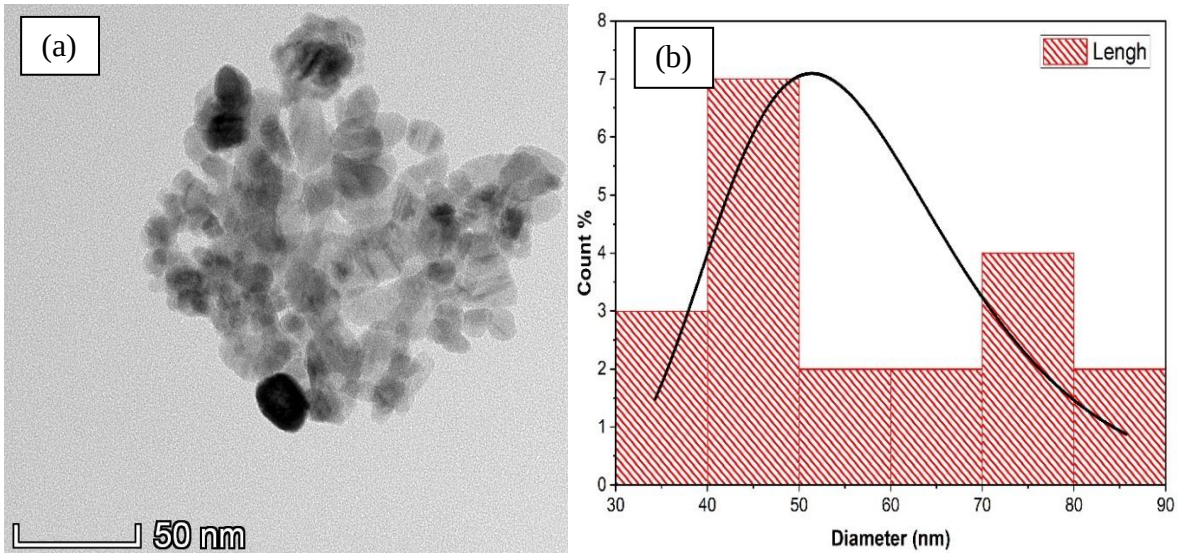

Fig 8. a) HR-TEM image b) Histogram of APL copper oxide nanoparticles

3.1.7 Dynamic Light Scattering (DLS)

To analyse the particles size distribution, green synthesized CuONPs were subjected to dynamic light scattering (DLS) analysis. DLS is an extensively used technique for determining the hydrodynamic diameter of nanoparticles established on the Brownian movement of particles in the suspension. The average hydrodynamic size of the nanoparticles Fig. (9) calculated by DLS is quite larger than the theoretical size of the nanoparticles calculated using XRD [46]. The variation in the nanoparticle size could be associated with the polydispersity index (PDI) values in turn related to the existence of nanoparticles as aggregates or agglomerates. PDI measurements were found to be 0.216 of APLCuONPs respectively. The PDI value revealed that the produced copper oxide nanoparticles monodispersed.

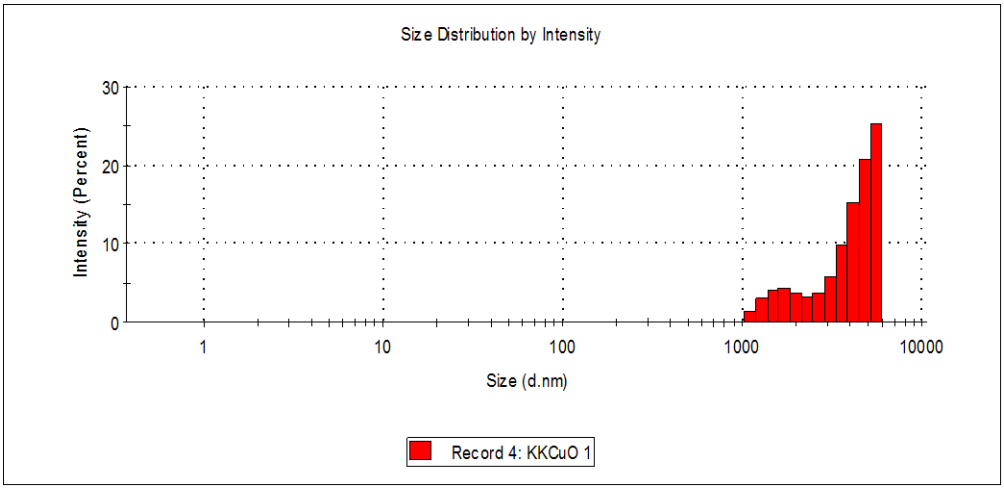

Fig. 9. DLS analysis of CuONPs from APL extract

3.2 Effect of Adsorption process parameters on removal of MR

3.2.1 Effect of initial dye concentration of MR

The inference of the initial concentration of MR in the Solutions on the rate of adsorption on CuONPs was investigated. The Experiments parameter was carried out with fixed adsorbent dosage optimal pH and stably maintained temperature. The percentage removal of MR is plotted against the initial dye concentration shown in Fig (10). The percentage removal of dye increased from 97.11to 98.43% with an increase in initial dye concentration from 10 to 50 mg/L, after that the adsorption efficiency decreased with increase dye concentration from 50 to 70 mg/L. Maximum adsorption of 98.43% was recorded for (50mg/L). This could be attributed to the increase in the driving force from higher concentration which enhances the sorption process.

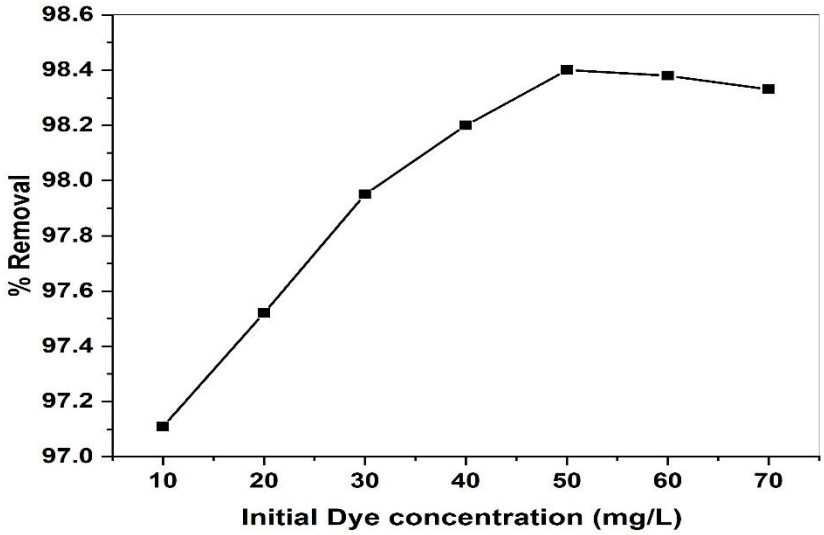

Fig.10.Effect of Initial MR dye concentration on the adsorption of GS-APLCuONPs.

3.2.2 Effect of Adsorbent Dosage

The effect of adsorbent dosage on the removal of the MR from aqueous solution was determined using variable quantities of GS- APLCuNOPs adsorbent ranging from 0.2 g to 1.0 g at fixed volumes 50 (ml) with initial dye solution 50 mg/L under constant parameters. The results are shown fig (11). The highest percentage of MR removal was achieved using 0.2g CuONPs. At elevated levels of CuONPs the amount of MR removal gets decreased. The observed decrease in MR dyes removal with increase adsorbent dosage from 99.21% to 97.85%. This phenomenon attributes to overlapping or aggregation of adsorption sites resulting in an increase total adsorbent surface area with respective initial dye concentration.

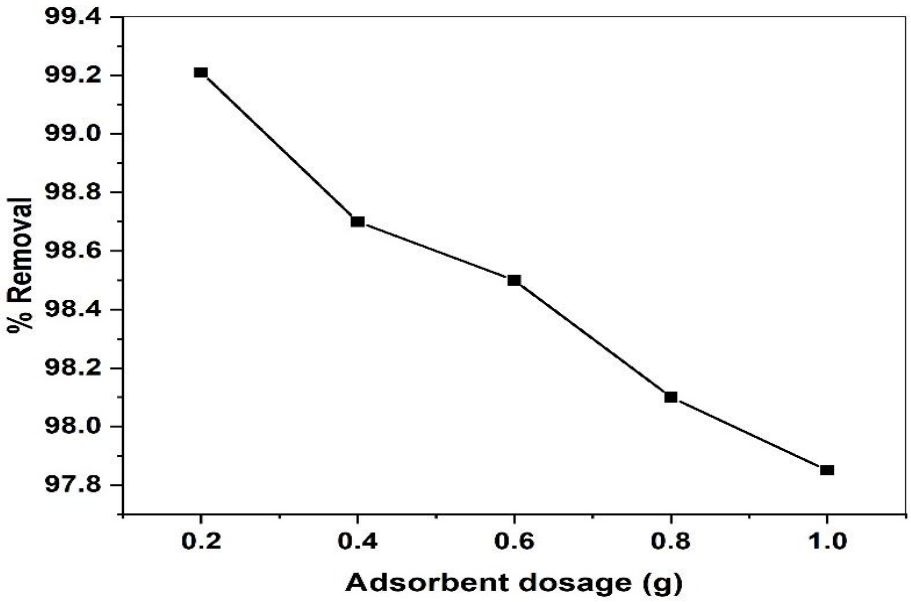

Fig 11. Effect of adsorbent dose on removal of methyl red

3.2.3 Effect of pH

To study the effect of initial pH onto adsorption. The pH of MR solution was varied from 3 to 8. The results of the variation in MR percentage removal with increase in pH is shown fig (12). As the solution pH was increased 3 to 5 the percentage removal of MR increased 97.88 to 99.08 % for CuONPs, after that the adsorption efficiency decreased. uptake of dyes mainly depends upon pH of adsorbent and PKa of the dyes. The pH of CuONPs found to be slightly acidic since its surface filled with positive charged particles. The PKa of MR is 5.1 [47]. The MR molecules are positively charged at PH>PKa. The increase in the percent dye removal with increase in pH from 3 to 5 for CuONPs might be ascribe to the electrostatic attraction between positively charged adsorbent surface and negatively charged dye molecules [48]. An increase pH beyond 5 for CuONPs percent removal decreased probably due to electrostatic repulsion between negatively charge adsorbent surface and positively charge dye molecules.

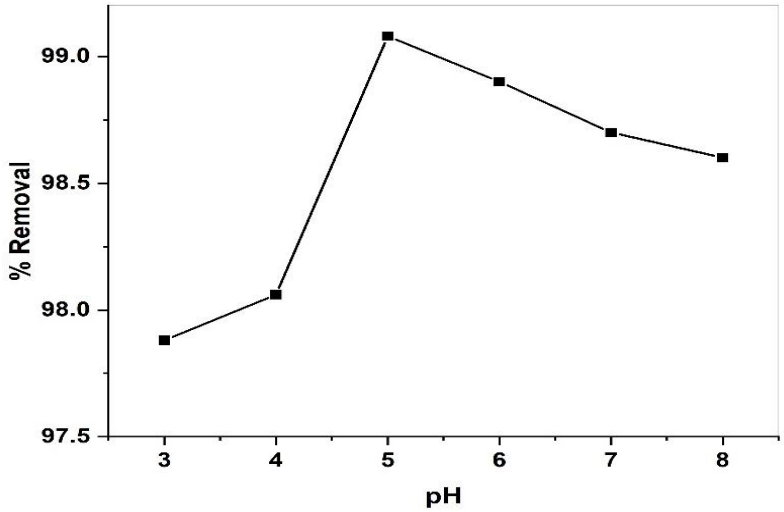

Fig 12. Effect pH on the adsorption of MR onto GS-APLCuONP

3.2.4 Effect of contact time :-

To identity the effect of contact time an experiment was conducted by mixing 50 ml of methyl red solution 50 mg/l concentration with 0.2g of GS-APLCuONPs adsorbent at constant pH 5 with varying time intervals of (30,60,90,120 and 150) minutes respectively. The contact time effect on the methyl red adsorption onto GS-APLCuONPs is depicted in fig (13). Which correlate relation between the percentage adsorption and adsorption time. The figure shows that the removal efficiency is equilibrium time dependent. It is evident that the amount of adsorption is rapid in the initial stages and decrease with increase in contact time. The fact which is inferred from the above process state large number of vacant sites were available for adsorption moment equilibrium attained at particular contact time due to desorption removal get decreased furtherly

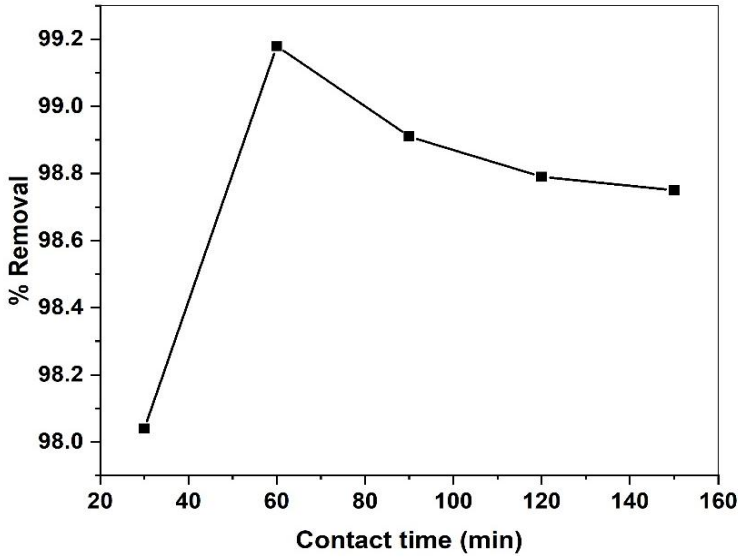

Fig 13. Effect of contact time on the adsorption of MR onto GS-CuONP.

3.2.5 Effect of temperature

Temperature is an important parameter that influence dye adsorption the effect of temperature on the percentage removal of methyl red onto GS-APL CuONPs is shown in fig (14). The percentage removal adsorption decreased from 99.01% to 98.16% with the temperature increased from 298K to 328K. This decrease in adsorption efficiency with increase in temperature maybe attributed mainly to the fact that the physical bonding between the dye (adsorbate) and the active sites of the adsorbent is weakness as the temperature rises. Furthermost the dye solubility increases also causing the interaction between the solute and solvent to become stronger than between the solute and adsorbent. This therefore makes it more difficult for the solute (i.e dye) to adsorb [49].

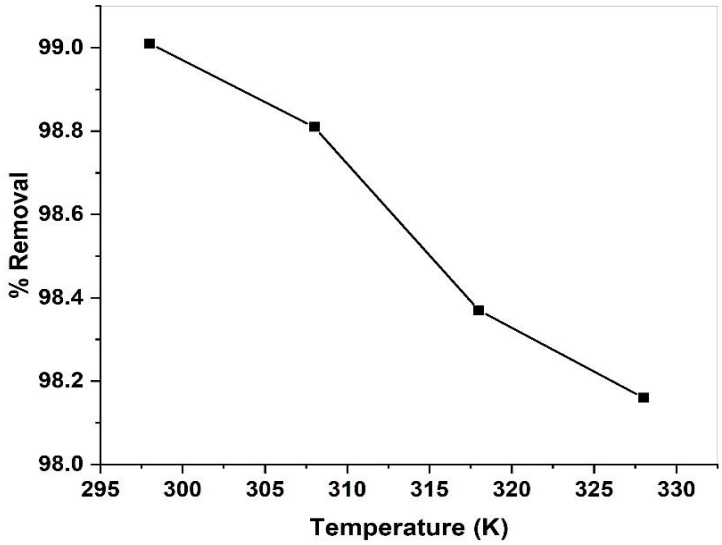

Fig 14. Effect of temperature on the adsorption of MR onto GS-APL CuONP

3.3 Adsorption isotherms

An adsorption isotherm indicates how adsorbed molecules distribute between the liquid phase and the solid phase when the adsorption process reaches an equilibrium state. The analysis of the isotherm data by fitting then to different isotherm models is an important step to find the suitable model that can be used for design purposes [50]. In the present experimental work, the isothermal results were analysed using well known expression for Langmuir Freundlich and Temkin isotherms. The applicability of the isotherm models to the adsorption study done was compared by judging the correlation coefficient R^2 values.

Langmuir isotherm

Langmuir adsorption model maximum adsorption corresponds to a saturated mono layer of the solute molecules on the adsorbent surface. Langmuir isotherm model assumes the uniform energies of adsorption onto the surface and no transmigration of adsorbate in the plane of the surface. Langmuir adsorption model based on the physical hypothesis that there is no interaction between adsorbed molecules and the adsorption energy over the entire coverage surface. Also, there is no transmigration of the adsorbate in the plane of the surface of the adsorbent [51]. Expression of the model is given by equation (4)

$$\frac{1}{qe} = \frac{1}{qmKlCe} + \frac{1}{qm} \qquad \text{Eq. (4)}$$

Where q_e is the amount of adsorbed dye at the equilibrium (mg g^{-1}), K_L (L mg^{-1}) and q_m (mg g^{-1}) are Langmuir constant related to energy adsorption and maximum adsorption capacity respectively. A graph was plotted $1/q_e$ against $1/c_e$ results in a straight lion with a slope of $(1/q_m)$ and intercept $(1/q_m)$.

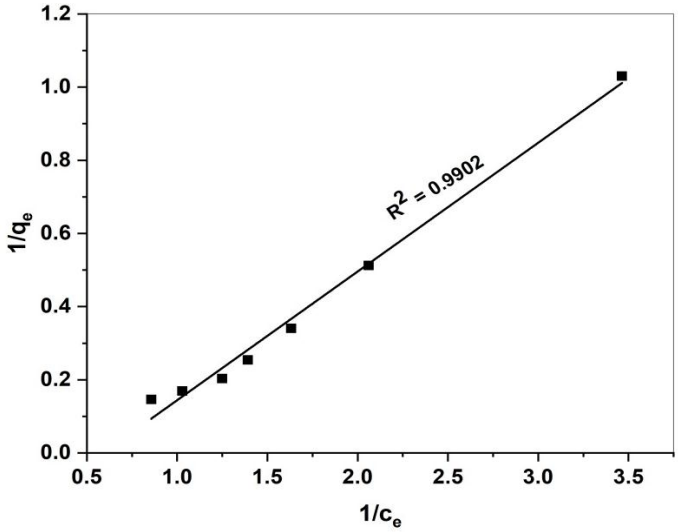

Fig 15. Langmuir isotherm plot for the adsorption of MR onto GS-APL CuONP

The essential characteristic of the Langmuir isotherm can be expressed in term of dimensionless constant separation factor R_L that is given equation (5).

$$R_L = 1/\ 1+K_LC_0 \qquad \text{Eq. (5)}$$

The values of R_L indicates the type of isotherm to be either favourable ($0 < R_L > 1$), unfavourable ($RL > 1$), linear ($RL = 1$) or irreversible ($RL = 0$). The values of R_L were found to be 0.03 suggesting the isotherm to be favourable at the concentration studied.

Freundlich isotherm

The Freundlich model is described by a formula Assuming heterogeneous multilayer adsorption on heterogeneous Surfaces. The Freundlich model also assumes interaction between the Adsorbates and that adsorption capacity increases with the analyte Concentration. The formula describing the Freundlich model is shown [52]

$$\log q_e = \log K_F + 1/n \log C_e \qquad \text{Eq. (6)}$$

Where K_F is the reaction constant reflecting adsorption Capacity (in 1 mg-1), and 1/n indicates dimensionless exponent of the Freundlich model to show adsorption intensity (it is calculated from the slope and intercept of log qe versus log Ce plot).

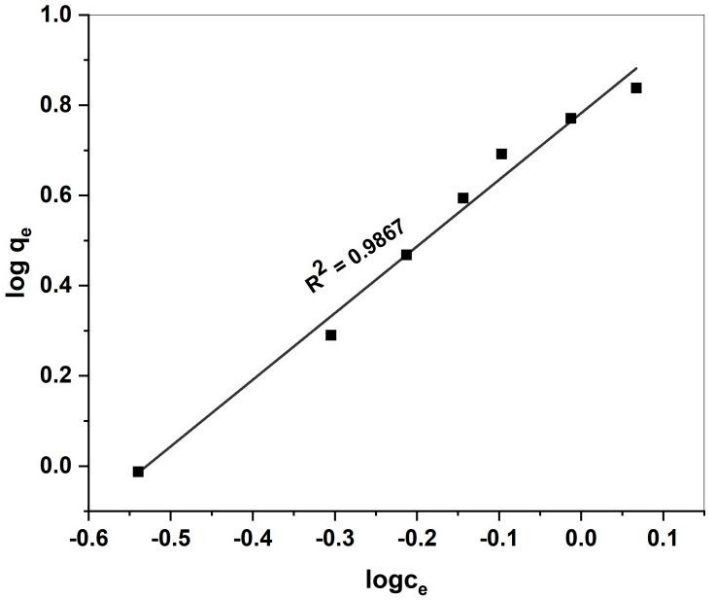

Fig 16. Freundlich isotherm plot for adsorption of MR onto GS-APL CuONP

Temkin isotherm

The Temkin isotherm model assumes that the Adsorption energy decrease linearly with the surface coverage due to adsorbent-adsorbate interaction. The linear form of Temkin Isotherm model is described as follows [53]

$$q_e = \frac{RT}{BT} lnKT + \frac{RT}{BT} ce \qquad \text{Eq. (7)}$$

Where BT is the Temkin constant related to the heat of sorption (KJ/mol), KT is the equilibrium binding constant Corresponding to the maximum binding energy (L/g), T is the Absolute temperature(K) and R is the gas constant (8.314×10^{-3} KJ/mol K).

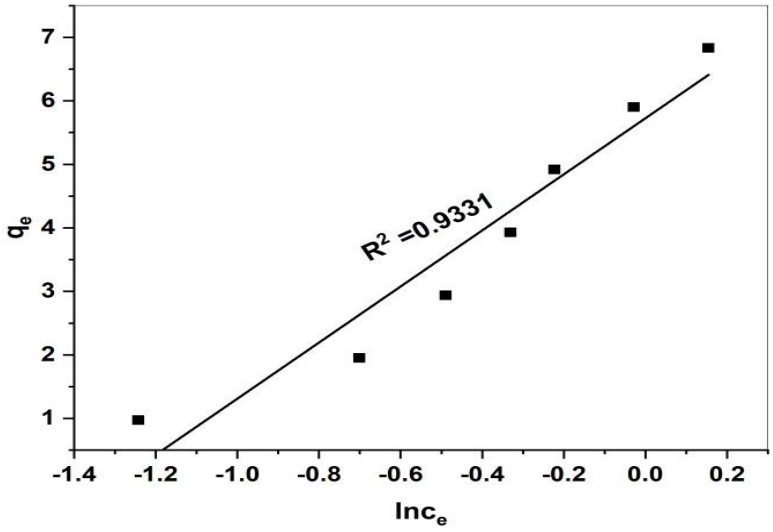

Fig 17. Temkin isotherm plot for the adsorption of MR onto GS-APL CuONPs

Fig 15,16, and 17., displays the Langmuir, Freundlich, and Temkin isotherms for our adsorption experiments. The calculated parameters for the all isotherms along with R^2 values are shown table (2).

Table (2). Isotherm parameters for removal of MR adsorption onto GS-APLCuONPs

Adsorption Isotherm	Parameters	Methyl Red
Freundlich Isotherm	K_F (mg/g)	6.0589
	1/n	1.4781
	n	0.6765
	R^2	0.9868
Langmuir Isotherm	K_L (mg^{-1})	0.5908
	q_m (mg/g)	4.8100
	R_L	0.0327
	R^2	**0.9902**
Temkin Isotherm	K_T (mol/g)	3.0024
	B_T (mol/kJ)	4.4789
	R^2	0.9331

The Langmuir isotherm model well fitted and good agreement with experimental data better than Freundlich and Temkin isotherm models. The results also confirmed by the high R^2 value for the Langmuir model (0.9902) compared with Freundlich (0.9867) and Temkin (0.9331) isotherm models. The Langmuir isotherm fit well because homogeneous distribution of active sites onto GS-CuONP surface. This finding was similar to other studies on the sorption of MR dye on different sorbent

3.3.2 Adsorption Kinetics studies

Adsorption kineties studies the relationship between adsorption capacity and reaction time. Thus, its main concern is adsorption speed dynamic equilibrium mass transfer and diffusion rates. Analysis of these parameters helps to understand adsorption process rates as well as adsorption mechanism. The pseudo-first-order model and pseudo-second-order model were used to investigate the adsorption kineties of the MR dye on GS-CuONPs.

The liner form of the pseudo-first-order kinetin model is represented by the following equation.

$$\text{Log } (q_e\text{-}q_t) = \log q_e - K_1/2.303.t \qquad \text{Eq (8)}$$

Where qe and qt are the values of amount of the dye adsorbed per unit mass on the adsorbent at equilibrium at various time respectively. K1 is the pseudo first order adsorption rate constant (min-1). The values of K1 and the calculated of are determined from slope and intercept respectively of the liners plot of log (qe-qt) versus t. Fig 18. where the values are given in table (3).

The liner form of the pseudo-second-order model is given by equation (9) [54]

$$t/qt = 1/K_2\, q_e^2 + t/q_e \qquad \text{Eq (9)}$$

Where K2 is the pseudo-scond-order adsorption rate constant (g/mg 1min) and qe is the amount of dye adsorbed (mg/g) on the adsorbent equilibrium. The initial adsorption rate (h = mg g^{-1}) is expressed as

$$h = K_2 qe^2$$

The plot of t/qt versus t gives a liner relationship which allows computation of K2 h and calculated qe shown fig 19.

The kinetic adsorption results of MR by GS-CuONPs under various condition from the related plots and the results are listed in table (2). The applicability of these model is based on the judgment on the respective correlation coefficient (R^2) and agreement between the experimental and calculated value of qe. The correlation coefficient R^2 (0.6029) values obtained for pseudo-first-order kinetic model were relatively low hence this model has very poor correlation coefficient for the fit data.

The pseudo-second-order rate constant K_2 and qe determined from the model as well as correlation coefficient presented in table (3). The observed R^2 (0.9950) values are very high for the pseudo-second-order kinetic model, where the values of qe_{cal} are good agreement with qe_{exp}. It is therefore evident that pseudo-second-order model is the best fit kinetic model in describing the adsorption process MR onto GS-CuONPs.

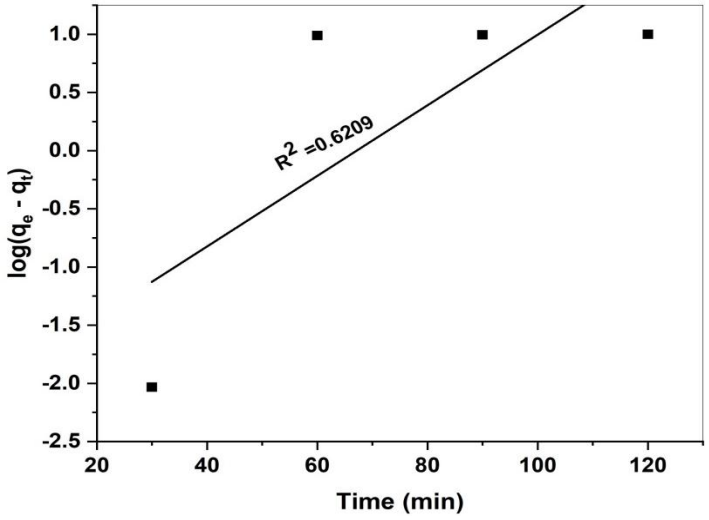

Fig 18. Pseudo-first-order kinetic model plot for adsorption of MR onto GS-CuONP

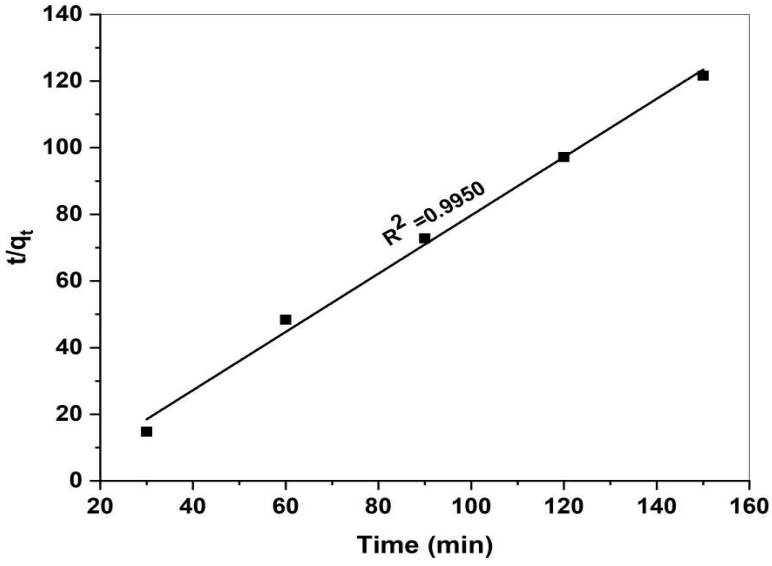

Fig 19. Pseudo-second order kinetic model for adsorption of the MR onto GS-CuO

Table 3. Adsorption kinetics of MR

Adsorption Kinetics	Parameters	Methyl Red
Pseudo First Order	K_1 (min^{-1})	0.0697
	q_e ($mg\ g^{-1}$)	5.8036
	R^2	0.6029
Pseudo Second Order	h ($g^{-1}\ mg^{-1}\ min^{-1}$)	0.1286
	q_e ($mg\ g^{-1}$)	1.1435
	R^2	0.9950

3.3.3 Thermodynamics

Thermodynamic parameters are important in adsorption studies they provide a better understanding of the effect of temperature on the adsorption process. The standard changes in Gibb's energy (ΔG^0) enthalpy (ΔH^0) and entropy (ΔS^0) were calculated using the following

$$\Delta G^0 = -RT\ln K \quad \text{Eq. (10)}$$

$$\log K = \Delta S^o/2.303\ R - \Delta H^o/2.303\ RT \quad \text{Eq. (11)}$$

Where R is the universal gas constant (8.314 J) T is the absolute temperature (k) and K is the equilibrium constant. Plots of ln K vs 1/T should be a straight line as shown in fig (20).

All thermodynamic parameters were tabulated in table (4). ΔG^o values were negative at all temperature studies. During the adsorption process the negative values of ΔG^o for the experimental temperature indicate spontaneous and favourable MR adsorption onto the surface of GS-CuONPs.

The negative enthalpy (ΔH^o) values obtained indicate the adsorption process was exothermic in nature. The positive entropy change (ΔS^o) values of corresponds to an increase in randomness occurred at solid-solution interface during the adsorption process. This is indirectly showing the affinity of adsorbent towards dye molecules [55].

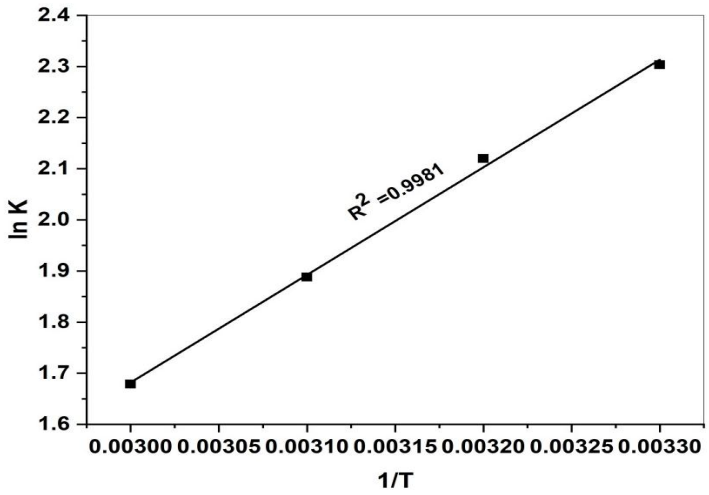

Fig 20. Thermodynamic parameter plot for the adsorption of MR onto GS-CuONPs

Table(4).Thermodynamic parameters values for adsorption of MR onto GS-APLCuONPs

Temperature (K)	ΔG^o (J.mol^{-1})	ΔH^o (KJ.mol^{-1})	ΔS^o (J.mol^{-}K^{-1})	R^2
298	-5.7063	-40.2875	88.6589	0.9981
308	-5.4281			
318	-4.9915			
328	-4.5788			

Conclusion

In this study, an eco-friendly and convenient green method from copper chloride dihydrate solution using Adenanthera Pavonina leaves extract was developed. The green synthesized copper oxide nanoparticles were confirmed by UV-vis, XRD, FT-IR, SEM-EDX, TEM and DLS. The synthesized copper oxide nanoparticles can be used as a promising catalyst for the removal of methyl red dye. The adsorption parameters such as initial dye concentration, Adsorbent dosage, pH, contact time, and Temperature also studied. The adsorption showed that the adsorption was best fitted to the Langmuir isotherm model as compared to the Freundlich and Temkin isotherm model. The rates of sorption were best fitted the pseudo second order kinetics. Thermodynamic study showed the spontaneous and exothermic in nature of biosorption process due to negative values of free energy change and negative values of enthalpy change. It was concluding this research found that the copper oxide nanoparticles with high dye adsorption capacity and good alternative for the removal of methyl red dye from aqueous solution very effectively.

References

1. Environmental Protection Agency, "*Nanotechnology white paper*," USEPA 100/B-07/001, 2007.

2. K. N. Thakkar, S. S. Mhatre, and R. Y. Parikh, "Biological synthesis of metallic nanoparticles," *Nanomedicine,* vol, no. **2**, 257-262 2010

3. Chen, H.; Roco, M. C.; Li, X, Lin, Y.-L. Trends in nanotechnology patents. *Nat. Nanotechnol.* 2008, **3**, 123-125.

4. Altikatoglu, M.; Attar, A.; Eric, F.; Cristache, C.M.; Isildak, I. Green synthesis of copper oxide nanoparticles using Ocimum basilicum ectract and their antibacterial activity. *Fresenius Environ. Bull.* 2017, **25**, 7832-7837.

5. R. G. Chaudhuri, S. Paria Core / shell nanoparticles. Classes properties, nanoparticle mechanism, characterization and applications. *Chem. Rev.* **112** (4) (2012) 2373-2433.

6. Lee Jackson, dirty Old London: The Victorian Fight Against Filth (2014)

7. John Tarantino. "Environmental Issues". The Environmental Blog. Archived from the original on 2011,12,10.

8. Udiba U.U. Gauje, B., Ashade, N.O., Ade-Ajayi, F.A. okezie V.C., Aji B.M., and Agboun, T.D T., 2014. An assessment of the heavy metal status of River Galma around Dakace industrial layout, Zaria, Nigeria,. *Merit Research Journal Of Environmental Science and Toxicology* 2 (8): 176-184

9. M. N. Ahmed, R.N. Ram, Removal of basic dye from wastewater using silica as adsorbent, *Environ. Pollut.,* **77**(1992) 79-85

10. W. A. Al-Amrani, P.E. Lim C.E. Seng, W.S. Wan Ngah, Bio regeneration of azo dyes-loaded monoamine modified silica in batch system: Effect of particle size and biomass acclimation condition, *Chem Eng.j.* **251** (20140 175-182.

11. S. Mondal, Methods of dye removal from house effluent- An overview, Environ. *Eng. Sci*. **25** (2008) 383-396

12. V, Larrechi MS, Callao MP (2007) kinetic and adsorption study of acid dye removal using activated carbon. Chemosphere **69**: 1151-1158.

13. Gupta VK, Kumar R, Nayak A, Saleh TA, Barakat MA (2013) Adsorptive removal of dyes aqueous solution onto carbon nanotubes: a review. *Adv Colloid Interface Sci* 193-194: 24-34.

14. Hassan, A.A and Abdulhussein, H. 2015. Methyl Red Dye Removal from Aqueous Solution by Adsorption on Rice Hulls. *Journal of Babylon University*, **3**: 23

15. Mas Rosemal H. Mas Haris and Kathiresan Sathasivam (2009). The Removal of Methyl Red from Aqueous Solutions Using Banana Pseudostem Fibers.

16. Laxmi, V. 2014. Removal of malachite green dye from water using orange peel as an adsorbent. Master of Technology Dissertation, *National Institute of Technology*, India.

17. Ferdous, J. Zainal-Abedin, Hafizur-Rahman and M-Ali-Hossain. 2014. Decolorization of Methyl Red by Hog Plum Peel and Sunfix Red by Bacterial Strains. *International Journal of Chemical and Environmental Engineering*. **5**(1):66-68.

18. NEILSEN LF., MOE D., KIRKEBY S., GARBARSCH C. Sirius red and acid fuchsin staining mechanisms. *Biotechnic Histochem.*, **73**, 71, 1998.

19. ZOBIR BIN HUSSEIN M., YAHAYA AH., SHAMSUL M., SALLEH HM., YAP T., KIU J. Acid fuchsin-interleaved Mg-Al-layered double hydroxide for the formation of an organic-inorganic hybrid nanocomposite. *Mater. Letter*, **58**, 329, 2004.

20. Dash Bibek, "Competitive Adsorption of dyes (congo red, methylene blue, malachite green) on Activated Carbon", 2011.

21. M. Q. Zhu, L. Zhu, J. J. Han, W. Wu, J.K. Hurst, A.D. Li, Spiropyranbased Photochromic polymer nanoparticles with optically switchable luminescence *J. Am. Chem.Soc*. **128** (13) (2006) 4303-4309.

22. K. Ulbrich, K. Hola, V. Subr, A. Bakandritsos, J. Tucek, R. Zboril, Targeted drug delivery with polymers and magnetic nanoparticles: covalent and noncovalent approaches, release control, and clinical studies, *Chem Rev*. **116** (9) (2016) 5338-5431.

23. S. M. Dhoble, N.S. Kulkarni Investigation of in vitro and involve antifungal property of biological synthesized copper oxide nanoparticles against rhizoctonia solani a phytopathogen of soyabean (Glycine max L. Merrill) *Int. J. Eng. Sci*. **4** (5) (2018) 17-30

24. V. K. Gupta Application of low-cost adsorbent for dye removal-A review, *J. Environ*. Manage. **90** (2009) 2313-2342.

25. A. Mittal, use of the hen feathers as potential adsorbent for the removal of a hazardous dye Brilliant Blue FCF from wastewater, *J. Hazard. Mater.* **128** (2006) 233-239.

26. B. Acemioglu, "Adsorption of Congo red from aqueous solution onto calcium-rich fly ash." *Journal of colloid and Interface Science,* vol. **274** (2), (2004) 371-379.

27. A. Maleki, B. Shahmorads solar degradation of Direct Blue 71 using surface modified iron doped ZnO hybrid nanoparticles, *water Sci. Water Treat*. **65** (2012) 1923-1928.

28. V. K. Gupta, A. Mittal, L. Kirshnan, and V. Gajbe, "Adsorption kinetics and column operation for the removal and recovery of malachite green from waste water using bottom ash." *Separation and purification technology,* **40** (1) (2004) 87-96.

29. D. S. Kim and B. Y. Park, "Effect on the removal Pb^{2+} from the aqueous solution by crab shell," *Journal of Chemical technology and Biotechnology*, **76** (11) (2001) 1179-1184.

30. S. R. H. Ghoreishi, Chemical catalytic reaction and biological oxidation for treatment non-biodegradable textile effluents *Chem. Eng. J*. **95** (2003) 163-169

31. Y.S. Ho, G. Mckay, Sorption of dyes and copper ion onto bio sorbent process Biochem. **38** (2003) 1047-1061.

32. K. Bhattacharyya, A. Sarma, Adsorption characteristic of the dye Brilliant Green on Neem leaf powder dyes pigm. **57** (2003) 211-222.

33. H. Daraei, A. Mittal, M. Noorosepehr, J. Mittal, separation of chromium from water sample using eggshell powder as a low-cost sorbent. Kinetic and thermodynamic studies, *Desalin. Water Treat.* **53** (2015) 214-220.

34. G. Sharma, M. Naushad, D. Pathania, A. Mittal, G. E. El-desoky, modification of Hibiscus Cannabinus fibre by graft copolymerisation: Application of dye removal, *Desalin. Water Treat.* **54** (2015) 3114-3121.

35. A. Mittal, Adsorption kinetics of removal of a toxic dye, Malachite green from wastewater by using hen feather, *J. Hazard. Matter*. **133** (2006) 196-202.

36. J. Mittal. V. Thakur, A. Mittal, Batch removal of hazardous azo dye Bismarck Brown R using waste material hen feather. *J. Ecol. Eng.* **602** (2013) 249-253.

37. Adowei, P., Horsfall jnr M. and Spiff A. I., 20212, "Adsorption **of** Methyl Red from Aqueous Solution by Activated Carbon produced from Cassava (Manihot esculenta Cranz) Peel Waste" *Innovation in Science and Engineering* **2**,24-33.

38. Azhar,S. S,Liew A.G., Suhardy, D., Hafiz, K. F, Hatim,M. D. I., 2005, "Dye Removal from Aqueous Solution by using Adsorption on Treated Sugarcane Bagasse", *American Journal of Applied Sciences* **2** (11): 1499-1503.

39. Long – Bao Shi, Pei-Fu Tang, Wei Zhang, Yan-Peng Zhao, Li-chang Zhang and Hao Zhang. Green synthesis of copper oxide nanoparticle using cassia auriculata leaf extraxt and vitro evaluation of their bio compatibility with rheumatoid arthrites macrophages. *Tropical Journal of Pharmaceutical Research*. January 2017; **16** (1): 185-192

40. R Chowdhury, N. Barah and M. H. Rashid, Facile biopolymer assisted synthesis of hallow SnO_2 babostructures and their application in dye removal, *ChemistrySelect,* 2016, **1**, 4682-4689.

41. Kavitha R. Francisca P. Anxilia A. Biosynthesis characterization and antibacterial effect of plants mediated silver nanoparticles from Adenanthera Pavonina Leaves. JETIR February 2019, vol **6**. (2)

42. D. Berra, S. Laouinia, B. Benhaouab, M. Ouahrania, D. Berrania and A. Rahald, "Green Synthesis of Copper Oxide nanoparticles by phoenix dactylifera leaves extract" Digest *Journal Nanoparticles and Biostructure*. vol.**13** 1231-1238.

43. Maruthupandy, M., Zuo, Y., Chen, J. S., Song, J. M. Niu, H. L. Mao, C. J. Zhang, S. Y. Shen, Y. H. 2017. Synthesis of metal oxide nanoparticles (CuO and ZnO Nps) via Biological template and their optical sensor application. *Applied Surface Science,* **397**: 167-174.

44. S. M. Yedukar C. B. Maurya, P. A. Mahanwar. A biological approach for the synthesis of copper oxide nanoparticles by Ixora Coccinea Leaf extract. *Journal of Material and Environmental Science.* **8** (4) (2007) 1173-1178.

45. Naika, H. R. Lingaraju, K., Manjunath, K., kumar, D., Nagaraju, G., Suresh, D., Nagabhushana, H. 2015. Green synthesis of copper oxide nanoparticles using Gloriosa superba L. extract and their antibacterial activity. *Journal of Taibah university for Science*,
9: 7-12

46. M. D. Jayappa, C. K. Ramaiah, M. A. Pavan Kumar, D. Suresh, A. Prabhu, R.P. Devasya and S. Sheik, *Applied Nanoscience*, **10**, (2020) 3057-3074.

47. M. Azami, M. Bahram, S.Nouri, Central composite design for optimization of removal of the azo dye , Methyl red, from waste water using Fenton reaction, Curr*, Chem. Lett.* **2** (2013) 57-68.

48. 4. K. Singh, T.J.M. Sinha, S. Srivastava, Functionalized nanocrystalline cellulose: smart biosorbent for decontamination of arsenic, int. *J. Miner. Process*. **139** (2015) 51-63.

49. A. Ozcan et al., Modification of bentonite with a cationic surfactant: An adsorption study of textile dye Reactive Blue 19, J. *Hazard. Mater*. **140**(1) (2007) 173-179.

50. Tam, I.A.W., A.L. Ahmad and B.H. Hameed, 2008. Adsorption of basic dye using activated carbon prepared from oil palm shell: Batch and fixed bed studies, **225**: 13-28. DOI: 10.1016/J.DESAL.2007.07.005

51. 7. Langmuir, I., 1918. The adsorption of gases on plane surfaces of glass, mica and platinum. *J. Am. Chem. Soc*. **40**: 1361-1403. DOI: 10.1021/ja02242a004

52. Ghaedi M, Nasab, AG, Khodadoust S, Rajabi M, Azizian S. 2014 application of activated carbon as adsorbents for efficient removal of methylene blue: kinetics and equilibrium study. *J.Ind.Eng.Chem.* **20**, 2317-2324. (doi: 10.1016/j.liec.2013.10.007).

53. B. Kiran, A. Kaushik, Chromium binding capacity of *Lyngbya Putealis* exopolysaccharides. *Biochem.Eng.J* **38**.(2008) 47-54

54. Y.S. Ho, G. McKay, Sorption of dye from aqueous solution by peat, *Chem. Eng. J*. **70** (1998) 115-124.

55. Bello oS, Tan, Ts, Ahm,ad MA> Adsorption of removal brilliant violet-5R recative dye from aqueous solution by Coca pod husk-based activated carbon. Kinetic Equilibrium and thermodynamic studies. *Asia Pal Journal Chem Eng*. (2012) **7**: 378-388.